Sensors & Actuators: B. Chemical 297 (2019) 126700

Contents lists available at ScienceDirect

Sensors and Actuators B: Chemical

journal homepage: www.elsevier.com/locate/snb

Miniature interferometric humidity sensor based on an off-center polymer cap onto optical fiber facet

Oskar Arrizabalaga[a,*], Javier Velasco[b], Joseba Zubia[a], Idurre Sáez de Ocáriz[b], Joel Villatoro[a,c]

[a] Department of Communications Engineering, Escuela de Ingenieria de Bilbao, University of the Basque Country UPV/EHU, Plaza Ingeniero Torres Quevedo 1, E-48013 Bilbao, Spain
[b] Fundación Centro de Tecnologías Aeronáuticas (CTA), Miñano, Spain
[c] IKERBASQUE -Basque Foundation for Science, E-48011 Bilbao, Spain

ARTICLE INFO

Keywords:
Optical fiber sensors
Interferometers
Microsensors
Polymer cap
Humidity sensors

ABSTRACT

In this work, we propose an interferometric humidity sensor based on a polymer micro-cap bonded off-center on the polished end of a standard single mode fiber (SMF). In our sensor, the sensitive part is the micro-cap. In the interferometer fabrication process, we can adjust the misalignment between the core and the micro-cap. It allowed us to control the visibility of the interference pattern. In our device, water molecules absorbed by the polymer microcap causes changes in the height of the microcap. This results in measurable shifts of the interference pattern. The fabricated samples were tested in a calibrated climatic chamber in the range from ˜10 to ˜95% of relative humidity (RH). The sensitivity and resolution of our device was found to be 148 pm per %RH and 0.04% RH, respectively. The obtained results suggest that our sensors can be useful to monitor relative humidity (RH) in miniature spaces.

1. Introduction

Humidity measurements have relevant importance in many areas of applications including, for example, manufacturing processes, [1] breath monitoring [2–5], or meteorological studies [6]. Every of such application demands specific humidity sensors. Therefore, factors such as range of detection, stability, response and recovery times, sensitivity or accuracy must be tailored when designing a humidity sensor. In addition, cost, simple design, and small size of the sensor are also important.

The most mature technology to develop humidity sensors exploit changes in resistance or capacitance of a humidity-sensitive thin film. The material the film is made of, can be polymer, bio-material, metal oxide, ceramic, or 2D material [7–11]. The physical changes of the thin film induced by humidity are measured by means of electronic technology. Nevertheless, electronic humidity sensors have some drawbacks. For example, they cannot measure humidity levels less than 5%, have nonlinear behavior or hysteresis, and need regular calibration. Besides, electronic humidity sensors may not work or cannot be used in environments where electromagnetic fields are present.

As an alternative to well-established electronic humidity sensors, those based on fiber optics technology have been proposed. Fiber optic humidity sensors have important features such as electromagnetic compatibility, remote sensing and multiplexing capabilities. Additionally, fiber optic humidity sensors have miniature size and are lightweight. As optical fibers are insensitive to humidity, an intermediate hygroscopic material is usually necessary. Such material can be deposited on a section or on the tip of an optical fiber. In this manner, the guided light interacts with the hygroscopic material, which in turn is exposed to humidity. The changes induced by humidity to such material result in measurable changes of the guided light.

Optical absorption is a technique to detect humidity [12–15]. In this technique, the evanescent field of the guided light interacts with the hygroscopic material and the transmitted spectrum is monitored as a function of humidity. The main disadvantage of this technique is that power fluctuations of the light source or curvature in the optical fiber can be misinterpreted as humidity.

Long period gratings (LPGs) [16] coated with a humidity-sensitive material can also be used to detect humidity. In an LPG cladding modes are excited [17], such modes are highly sensitive to changes of refractive index of the material that coats the LPG [18]. Nevertheless, it is difficult to have full control of the cladding modes that are excited with an LPG, thus sensors based on LPGs have low yield [19–22].

Fiber Bragg gratings (FBG) [23] are also widely used to design and fabricate humidity sensors. The working principle of these sensors is based on changes in the Bragg wavelength of the FBG caused by the

* Corresponding author.
E-mail address: oskar.arrizabalaga@ehu.es (O. Arrizabalaga).

https://doi.org/10.1016/j.snb.2019.126700
Received 28 February 2019; Received in revised form 12 June 2019; Accepted 14 June 2019
Available online 17 June 2019

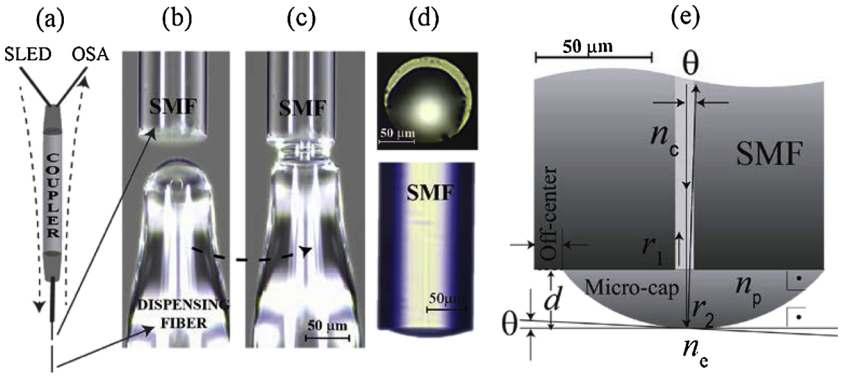

Fig. 1. (a) Schematic representation of the set-up used to monitor the fabrication process and to interrogate devices. (b) and (c) Micrograph of the fabrication steps where the polymer is added to the end face of the SMF.(d) Micrographs of a fabricated sensor sample. On top, frontal view of the off-center of the micro-cap. Below, lateral view of the sensor. (e) Illustration of the theoretical principle of our interferometer.

swelling of a hygroscopic material deposited around the segment of fiber that has the grating [24,25]. An important advantage of FBG sensors is their multiplexing capability. However, FBG humidity sensors have low sensitivity, narrow measuring range, and slow response time [26]. Since different materials possess different swelling properties, many materials have been proposed by different groups in an effort to improve the performance of such humidity sensors [27–29]. Also, different coating methods and thicknesses have also been studied with the aim to improve the sensitivity of FBG humidity sensors [30–32].

Interferometry is another technique widely used for humidity sensing. There are different ways to implement interferometers, as for example, with tapered optical fibers [33,34], photonic crystal fibers [35–37], or with a combination of different types of fibers [38,39]. The main characteristic of most interferometric humidity sensors is their cross sensitivity to humidity and to other parameters such as temperature. An advantage of interferometers is the fact that they can detect humidity even without a hygroscopic material [40]. Interferometric humidity sensors have also some disadvantages. These include low sensitivity to humidity and the narrow humidity range that they can measure [41–43].

Fabry-Perot (FP) cavities are also good alternatives to monitor humidity. In this case, a thin layer of hygroscopic material is deposited on the end face of an optical fiber [44–47]. The advantage of this type of humidity sensors is their miniature size. However, in most cases, the deposition of the material is carried out manually [43,48–51]. Thus, the reproducibility is low [48]. Many research groups have proposed different configuration of FP-based humidity sensors have to improve their performance [52,53], but the thermo-optic (TO) and thermo-expansion (TE) effects on the polymer have not been analyzed. On the other hand, FP-based humidity sensors that can compensate temperature effect, require an additional temperature sensor [49]. Therefore, despite the many advantages that humidity sensors based on optical fibers have, their characteristics must be improved to compete with their electronic sensors counterpart. These characteristic include simpler design and reproducible fabrication methods which may lead to lower sensor costs. Other important factor include high sensitivity and accuracy, wide measurement range, miniature size, no hysteresis, linear behavior, stability, etc.

Based on the aforementioned, in this work, we propose a miniature interferometric humidity sensor. The design of our device is simple which allowed us to achieve high reproducibility. As a hygroscopic material, we used nanoliter amounts of a UV-curable polymer (NOA 81 from Norland Products, Inc) that is commercially available. A simple setup was implemented to monitor the fabrication process in real time. In this manner, we achieved devices with well-defined interference patterns that were analyzed with a low cost spectrometer. In addition, in our devices, the effect of temperature on the polymer micro-cap can be compensated with another interferometer isolated from humidity [54].

According to the manufacturer, the polymer, once cured and aged, can withstand temperatures from −150 °C to 125 °C. Therefore, the devices here proposed are suitable for a myriad of environments or aplications. The fabricated samples were exposed to humidity from 10 to 95% at different temperatures. The obtained results show that our devices are highly sensitive to humidity (148 pm per %RH), are accurate and as fast as a commercial capacitive humidity sensor. In addition, the behavior of our sensor is linear over a broad range of humidity and has no hysteresis. An additional advantage of our humidity sensors is their microscopic dimensions.

2. Sensor fabrication process

The device fabrication consists of the following steps. Firstly, a standard single mode fiber (SMF) was cleaved using a fiber optic cleaver (model CT-32 from Fujikura). After that, the cleaved fiber was polished flat with a fiber optic polishing machine, model NOVA from Krell Tech. Once this was done, the SMF was cleaned and then clamped to an optical fiber alignment stage (ULTRAlign™ from Newport). Additionally, a short piece of cleaved SMF was submerged in a commercial polymer (NOA 81, from Norland Products). The polished and the cleaved SMFs were clamped is separated fiber alignment stages that were in vertical position. The SMF coated with polymer was placed beneath of the polished SMF. Next, light from a super luminescent diode (SLD) source, with peak emission at 850 nm, was launched to the polished SMF end by means of a suitable optical coupler. The interference pattern generated by the two SMF faces was analyzed using a mini spectrometer. Then, the SMF coated with polymer was approached to polished SMF tip until the spectrum from the air gap formed between the end face of the SMF and the polymer had a well-defined interference pattern, see Fig. 1(b).

After this, the fibers were misaligned. The next step was to gently move the dispensing fiber in the direction of the polished SMF until both fibers were in contact, see Fig. 1(c). Then, the dispensing SMF was moved downwards. As a result, an off-center micro-size polymer cap on the end face of the polished SMF was formed, see Fig. 1(d). Finally, to solidify the polymer cap, it was exposed to UV light during a few seconds. By the polymer manufacturer recommendation, for an optimum adhesion, the device was aged at 50 °C during 12 h. In Fig. 1(d), we show micrographs of the front and lateral views of the resulting polymer cap onto the polished SMF.

We would like to point out that the process described above can be carried out automatically. For example, similar opto-mechanical components (mini cameras, translation stages, etc.), techniques, and alignment process implemented in commercial fiber fusion splicers can be adopted to align the dispensing and receiving fibers. Therefore, the fabrication of the devices proposed here can be carried out in seconds.

3. Operation principle

The operating principle of our device is explained as follows. The

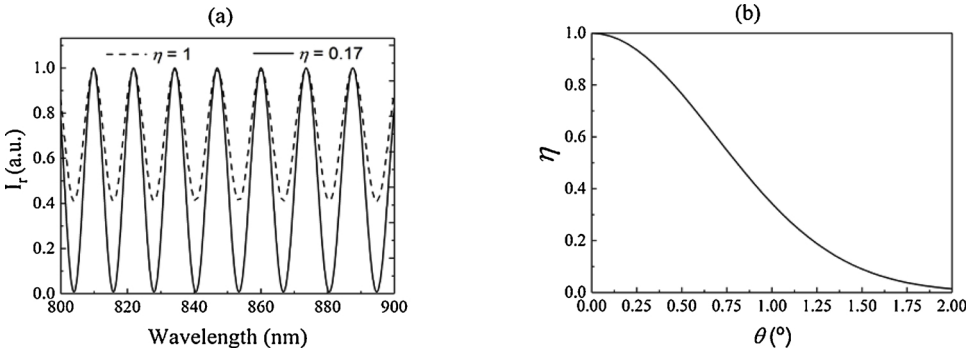

Fig. 2. (a) Theoretical simulation of our interferometric device, calculated from Eq.(5) with an angular misalignment of 1.26° and without angular misalignment, solid and dashed line, respectively. (b) Coupling coefficient versus axial misalignment.

fundamental SMF mode is considered as a Gaussian beam with amplitude E_0. Part of this beam, due to Fresnel reflection, will be reflected towards the SMF core once it reaches the SMF-polymer interface. The amplitude of the reflection is denoted as r_1, see Fig. 2(a). Therefore, the reflected wave, denoted as E_{r1}, can be expressed as:

$$E_{r1} = r_1 E_0, \tag{1}$$

where r_1 is the reflection coefficient and is calculated as $r_1 \approx (n_p - n_c)/(n_p + n_c)$. In the latter equation, n_p and n_c are the refractive index of the polymer and the core of the SMF, respectively. The non-reflected part of the wave will travel in the polymer until it reaches the polymer-SMF interface. As the beam is Gaussian, the waist radius of such a beam can be calculated as $w_1 = w_0[1 + (d\lambda/\pi n_p w_0^2)^2)]1/2$. The accumulated phase of the beam is given by the expression: $\phi = 2\pi n_p d/\lambda$. In the expressions of w_1 and φ, d is the height of the polymer microcap and λ the centered wavelength of the optical source, and is w_0 is the waist of the beam before leaving the SMF core.

After reaching the polymer-external medium interface, the wave will be reflected back due to the Fresnel reflection. The amplitude of the reflected beam can be mathematically written as:

$$E_{r2} = E_0 r_2 (1 - r_1) exp(-i\phi), \tag{2}$$

where r_2 is the reflection coefficient in the interface polymer-outside medium and is calculated as $r_2 \approx (n_e / n_p)/(n_e + n_p)$, being n_e the refractive index of the external medium. The waist radius of E_{r2} beam that reaches the SMF core can be denoted as ω_d. It can be expressed in a similar manner than w_1.

Due to the misalignment of the polymer-cap, the portion of the reflected wave that is coupled in the SMF core will be [55,56]:

$$E_c = \eta r_2 E_0 (1 - r_1)^2 \exp(-i2\phi), \tag{3}$$

where η is the coupling coefficient that can be calculated from Eqs. A7 and A(8) given in reference [55]. It depends strongly on the angular misalignment, θ, see Fig. 1(e). Thus, the amplitude of the total reflected wave (E_T) is the sum of E_{r1} and E_c, that it is:

$$E_T = E_0[r_1 + \eta r_2 (1 - r_1)^2 exp(-i\phi)]. \tag{4}$$

Therefore, the total reflected intensity that can be measured with a light detector can be expressed as $I_r = (E_T/E_0)^2$. The result of this operation turns out to be:

$$I_r = r_1^2 + \eta^2 r_2^2 (1 - r_1)^4 + 2\eta r_1 r_2 (1 - r_1)^2 \cos(2\phi). \tag{5}$$

It can be noted that Eq. (5) is not the typical expression assumed by most authors for Fabry-Perot interferometers [48,57] which is considered as a two beam interferometer. The divergence of the beam that leaves the SMF and the features of the interface of the polymer (or any other material) and the external medium determine the performance of the interferometer, hence of the sensor.

From Eq. (5) it is possible to deduce that the maximums of the I_r will be given when $\varphi = 2m\pi$ and the minimum when $\varphi = (2m + 1)\pi$, m being a positive integer. So, the wavelengths of the interference pattern where I_r takes maximum values will be located at:

$$\lambda_m = (2n_p d)/m \tag{6}$$

The visibility (V) of an interference pattern is defined as the difference over the sum between the maximum and minimum of such a pattern. Thus, from Eq. (5), we can derived V as:

$$V = \frac{4\eta(1 - r_1)\sqrt{r_1 r_2})}{2r_1 + 2\eta^2(1 - r_1)^2 r_2}. \tag{7}$$

From Eq. (7), it can be deduced that it is possible to achieve a maximum value of V by adjusting the coupling coefficient η, which depends on the axial misalignment θ, n_p, d, λ, ω_0, and w_d [55,58].

According to Eq. (5), the maximum value of V is found when the $\eta = 0.17$. This value was found by calculating η when $\theta = 1.26°$. We also have plotted Eq. (5) when $\theta = 0$, that is when $\eta = 1$. In Fig. 2(a), we have graphed the comparative of both mentioned situations. It can be seen that the visibility increases 40% due to the off-centering of the microcap. Fig. 2(b) shows the strong influence of the misalignment on the coupling coefficient η, and consequently, on the visibility of the interference pattern, see Eq. (7).

4. Experimental results

The polymer that we used to fabricate the micro caps onto the SMF can absorb water molecules [59]. Such polymer swells when it is exposed to relative humidity (RH). Consequently, the height of the microcap d, will increase if RH increases. Thus, our device can be used as a humidity sensor. According to Eq. (6) and, by assuming constant temperature, λ_m will shift to the red if d increases (RH increases), or will shift to the blue if the RH decreases.

Our devices were assessed as humidity sensors in the Aerospace Test Laboratory located in Miñano, Spain. To do so, the interrogation system shown in Fig. 1(a) was used. A broadband light from a super luminescent diode source (SLD), model OFLS- S from Safibra, was launched into the core of the SMF through a suitable optical coupler. By means of a mini-spectrometer (CCS 100 from Thorlabs), one of the maximum wavelengths (λ_m) of I_r, was tracked and analyzed. After that, our devices were placed inside of a calibrated climatic chamber (mode Climacell,- from MMM Group). A capacitive humidity sensor was used as a reference. The climatic chamber was programmed in order to subject our devices to different tests.

In Fig. 3(a), it can be seen the shift of the spectrum of one of our device when it was exposed to different concentration of RH at 22 °C. Note the good agreement between the experimental spectrum and the theoretically calculated spectrum shown in Fig. 2(a). Fig. 3(b) shows the response of our device when it was exposed to RH from ˜10 to ˜ 95% in steps of 15% and down to ˜10% in the same steps. It can be noted that our device provided information about RH as accurate as the electronic

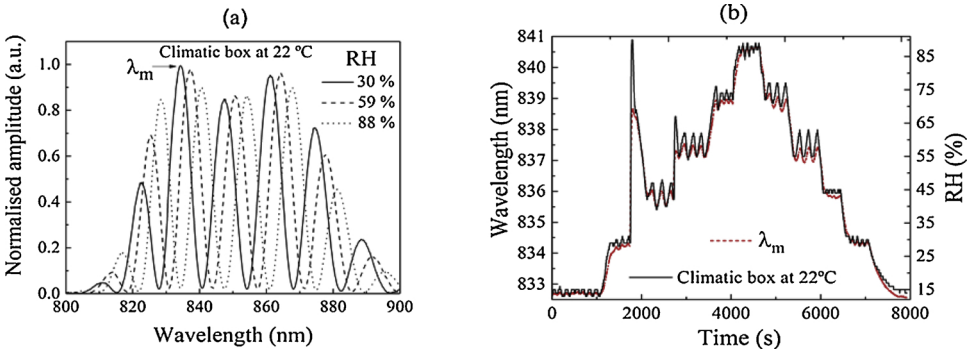

Fig. 3. (a) Spectra at different RH of our sensor, λ_m denotes the tracked maximum. (b) Comparative in real time between our device and the capactive humidity sensor of the calibrated climatic box.

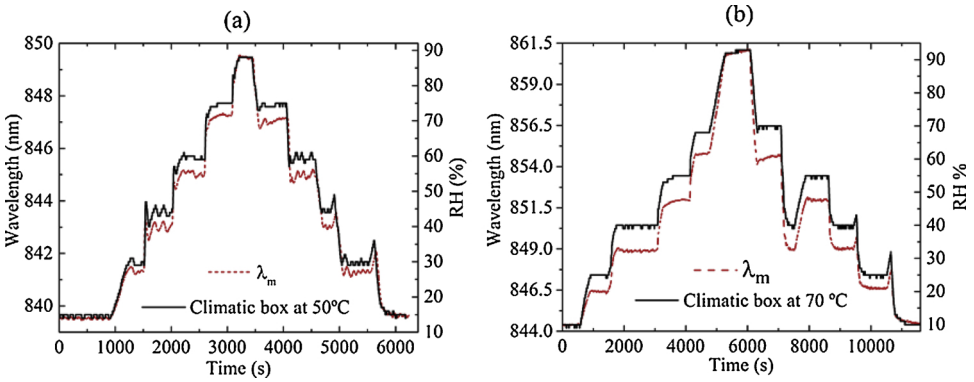

Fig. 4. (a) Comparative in real time between our device and the capactive humidity sensor of the calibrated climatic box at 50 °C. (b) The same comparative that the previous one but with the climatic box at 50 °C.

sensor located in the climatic chamber.

The aforementioned tests, were also carried out at 50 and 70 °C and the results obtained are shown in Figs. 4(a) and 4(b). These graphs show how the tracked wavelength (λ_m) of the spectrum, shifts to the red or to the blue according to the climatic chamber RH variations. From the data of the aforementioned graphs, our sensor was calibrated for each temperature test carried out. The result as summarized in Fig. 5(a). From the sensor calibration, it can be seen that our sensor behaves linearly and without hysteresis.

The response of our device to cycles of RH between 30 and 90% was also studied. The results are shown in Fig. 5(b). Note also that in this case of our device provides again accurate information as an electronic humidity sensor.

To compensate the temperature effect on our sensor we need to understand the response of the polymer micro-cap to temperature. By differentiating Eq. (6) with respect to temperature we get [54]:

$$\frac{\partial \lambda_m}{\partial T} = \left[\frac{1}{n_p}\frac{\partial n_p}{\partial T} + \frac{1}{d}\frac{\partial d}{\partial T}\right]\lambda_m. \tag{8}$$

This means that temperature will cause a shift to λ_m. Thus, to compensate the temperature effect on our devices will be necessary to use two SMF with polymer microcaps, one of them must to be isolated from humidity.

The effect of temperature on the maximum of the interference pattern (λ_m) and on the RH sensitivity (S_{RH}) is calculated according to the two following equations:

$$\lambda_m(T) = 827,6 + 0.254 \cdot T\,(\mathrm{nm/^oC}), \tag{9}$$

$$S_{RH}(T) = 0.148 - 0.0033 \cdot T + 5,9E-5 \cdot T^2\,(\mathrm{nm/\%RH}). \tag{10}$$

Furthermore, the resolution of our sensor was found to be 0.04% RH.

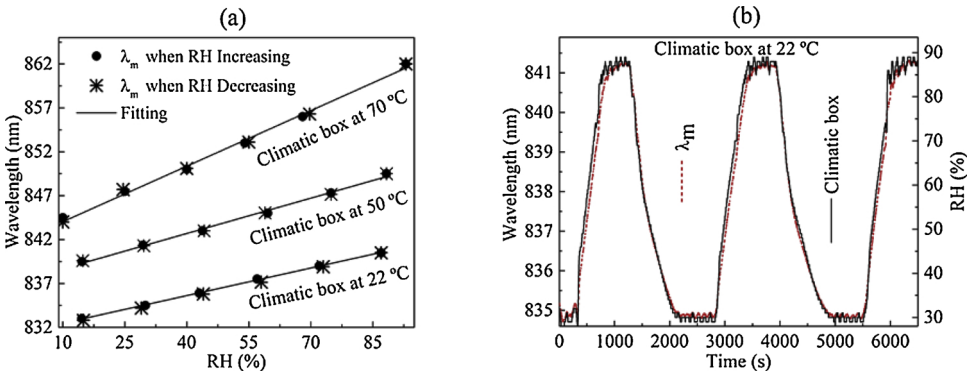

Fig. 5. (a) Plot of RH versus of λ_m at differents temperatures. At all temperatures the response of our sensor was linear and without hysteresis. (b) Response of our sensor when it is exposed to several cycles of RH variations from ˜30 to ˜90% at 22 °C.

5. Conclusions

We have reported on an accurate interferometric fiber optic humidity sensor which has miniature size. Experimentally, it has been shown to be as fast, accurate and sensitive as a commercial capacitive humidity sensor with which it has been compared. Our sensor provides linear response, broad humidity measuring range, and high sensitivity over the whole measuring range. The fabrication of the sensors is simple and reproducible. In our humidity sensor, the key element is an off-center polymer microcap bonded onto the polished facet of a single mode optical fiber. It can be possible compensate the temperature effect on the polymer by using two of our devices, one of them isolated from humidity.

We believe that the devices here proposed can be useful in miniature spaces where reliable and accurate humidity measurements are needed. Other applications that we foresee are in the field of bio-chemical sensing. In these applications, synthetized polymers with tailored optical and physical properties will be required. Then, under the presence of the parameters to sense, the interference pattern will change, and therefore will be detected or monitored with the techniques proposed in this work.

Acknowledgements

This work was funded by the Fondo Europeo de Desarrollo Regional (FEDER); the Ministerio de Economía y Competitividad (projects PGC2018-101997-B-I00 and RTI2018-094669-B-C31), and in part by the Gobierno Vasco/Eusko Jaurlaritza IT933-16 and ELKARTEK KK-2018/00078, (μ4Indust and SMARTRESNAK). Oskar Arrizabalaga acknowledges a PhD fellowship from the Departamento de Educación, Política Lingüística y Cultura del Gobierno Vasco/Eusko Jaurlaritza.

References

[1] W. Kastner, G. Neugschwandtner, S. Soucek, H.M. Newman, Communication systems for building automation and control, Proceedings of the IEEE 93 (6) (2005) 1178–1203, https://doi.org/10.1109/JPROC.2005.849726.
[2] T. Tatara, K. Tsuzaki, An apnea monitor using a rapid-response hygrometer, J. Clin. Monit. 13 (1) (1997) 5–9, https://doi.org/10.1023/A:1007380021895.
[3] B. Du, D. Yang, X. She, Y. Yuan, D. Mao, Y. Jiang, F. Lu, MoS_2-based all-fiber humidity sensor for monitoring human breath with fast response and recovery, Sens. Actuators B Chem. 251 (2017) 180–184, https://doi.org/10.1016/j.snb.2017.04.193.
[4] U. Mogera, A.A. Sagade, S.J. George, G.U. Kulkarni, Ultrafast response humidity sensor using supramolecular nanofibre and its application in monitoring breath humidity and flow, Sci. Rep. 4 (2014) 4103, , https://doi.org/10.1038/srep04103.
[5] C. Laville, C. Pellet, G. N'Kaoua, Interdigitated humidity sensors for a portable clinical microsystem, 1st Annual International IEEE-EMBS Special Topic Conference on Microtechnologies in Medicine and Biology - Proceedings (2000), https://doi.org/10.1109/MMB.2000.893849.
[6] W.P. Elliott, D.J. Gaffen, On the utility of radiosonde humidity archives for climate studies, Bull. Am. Meteorol. Soc. 72 (10) (1991) 1507–1520, https://doi.org/10.1175/1520-0477(1991)072<1507:OTUORH>2.0.CO;2.
[7] Y. Sakai, Y. Sadaoka, M. Matsuguchi, Humidity sensors based on polymer thin films, Sens. Actuators B Chem. 35 (1–3) (1996) 85–90, https://doi.org/10.1016/S0925-4005(96)02019-9.
[8] Z.-T. Zhu, J.T. Mason, R. Dieckmann, G.G. Malliaras, Humidity sensors based on pentacene thin-film transistors, Appl. Phys. Lett. 81 (24) (2002) 4643–4645, https://doi.org/10.1063/1.1527233.
[9] C.T. Wang, C.L. Wu, I.C. Chen, Y.H. Huang, Humidity sensors based on silica nanoparticle aerogel thin films, Sens. Actuators B Chem. 107 (1) (2005) 402–410, https://doi.org/10.1016/j.snb.2004.10.034.
[10] K.P. Yoo, L.T. Lim, N.K. Min, M.J. Lee, C.J. Lee, C.W. Park, Novel resistive-type humidity sensor based on multiwall carbon nanotube/polyimide composite films, Sensors and Actuators, B: Chemical. 145 (1) (2010) 120–125, https://doi.org/10.1016/j.snb.2009.11.041.
[11] W. Geng, X. He, Y. Su, J. Dang, J. Gu, W. Tian, Q. Zhang, Remarkable humidity-responsive sensor based on poly (N,N-diethylaminoethyl methacrylate)-b-polystyrene block copolymers, Sens. Actuators B Chem. 226 (2016) 471–477, https://doi.org/10.1016/j.snb.2015.12.027.
[12] Y. Xiao, J. Zhang, X. Cai, S. Tan, J. Yu, H. Lu, Y. Luo, G. Liao, S. Li, J. Tang, Z. Chen, Reduced graphene oxide for fiber-optic humidity sensing, Opt. Express 22 (25) (2014) 31555–31567, https://doi.org/10.1364/OE.22.031555.
[13] X. Peng, J. Chu, B. Yang, P.X. Feng, Mn-doped zinc oxide nanopowders for humidity sensors, Sens. Actuators B Chem. 174 (2012) 258–262, https://doi.org/10.1016/j.snb.2012.07.011.
[14] I.R. Matias, F.J. Arregui, J.M. Corres, J. Bravo, Evanescent field fiber-optic sensors for humidity monitoring based on nanocoatings, IEEE Sens. J. 7 (1) (2007) 89–95, https://doi.org/10.1109/JSEN.2006.886889.
[15] Z. Zhao, Y. Duan, A low cost fiber-optic humidity sensor based on silica sol-gel film, Sensors and Actuators, B: Chemical. 160 (1) (2011) 1340–1345, https://doi.org/10.1016/j.snb.2011.09.072.
[16] S.W. James, R.P. Tatam, Optical fibre long-period grating sensors: characteristics and application, Meas. Sci. Technol. 14 (5) (2003) R49–R61, https://doi.org/10.1088/0957-0233/14/5/201.
[17] O. Ivanov, S. Nikitov, Y. Gulyaev, Cladding modes of optical fibers: properties and applications, Physics-Uspekhi. 49 (2) (2006) 117–224, https://doi.org/10.1070/PU2006v049n02ABEH005784.
[18] L. Alwis, T. Sun, V. Grattan Kenneth, Analysis of polyimide-coated optical relative humidity sensor, IEEE Sens. J. 7 (2) (2013) 767–771, https://doi.org/10.1109/JSEN.2012.2227714.
[19] L. Alwis, T. Sun, K.T.V. Grattan, Fibre optic long period grating-based humidity sensor probe using a Michelson interferometric arrangement, Sensors and Actuators, B: Chemical. 178 (1970) 694–699, https://doi.org/10.1016/j.snb.2012.11.062.
[20] M. Konstantaki, S. Pissadakis, S. Pispas, N. Madamopoulos, N.A. Vainos, Optical fiber long-period grating humidity sensor with poly(ethylene oxide)/cobalt chloride coating, Appl. Opt. 45 (19) (2006) 4567–4571, https://doi.org/10.1364/AO.45.004567.
[21] X. Yu, P. Childs, M. Zhang, Y. Liao, J. Ju, W. Jin, Relative humidity sensor based on cascaded long-period gratings with hydrogel coatings and Fourier demodulation, Ieee Photonics Technol. Lett. 21 (24) (2009) 1828–1830, https://doi.org/10.1109/LPT.2009.2034620.
[22] D. Viegas, J. Goicoechea, J.L. Santos, F.M. Araújo, L.A. Ferreira, F.J. Arregui, I.R. Matias, Sensitivity improvement of a humidity sensor based on silica nanospheres on a long-period fiber grating, Sensors. 9 (1) (2009) 519–527, https://doi.org/10.3390/s90100519.
[23] K.O. Hill, G. Meltz, Fiber Bragg grating technology fundamentals and overview, J. Light. Technol. 15 (8) (1997) 1263–1276, https://doi.org/10.1109/50.618320.
[24] N.A. David, P.M. Wild, N. Djilali, Parametric study of a polymer-coated fibre-optic humidity sensor, Meas. Sci. Technol. 46 (7) (2012) 032001–037001, https://doi.org/10.1088/0957-0233/23/3/035103.
[25] P. Kronenberg, P.K. Rastogi, P. Giaccari, H.G. Limberger, Relative humidity sensor with optical fiber Bragg gratings, Opt. Lett. 27 (16) (2002) 1385–1387, https://doi.org/10.1364/OL.27.001385.
[26] T.L. Yeo, T. Sun, K.T.V. Grattan, D. Parry, R. Lade, B.D. Powell, Characterisation of a polymer-coated fibre Bragg grating sensor for relative humidity sensing, Sens. Actuators B Chem. 110 (1) (2005) 148–156, https://doi.org/10.1016/j.snb.2005.01.033.
[27] Y. Lin, Y. Gong, Y. Wu, H. Wu, Polyimide-coated fiber Bragg grating for relative humidity sensing, Photonic Sens. 5 (1) (2015) 60–66, https://doi.org/10.1007/s13320-014-0218-8.
[28] A.J. Swanson, S.G. Raymond, S. Janssens, R.D. Breukers, M.D.H. Bhuiyan, J.W. Lovell-Smith, M.R. Waterland, Development of novel polymer coating for FBG based relative humidity sensing, Sens. Actuators A Phys. 249 (2016) 217–224, https://doi.org/10.1016/j.sna.2016.08.034.
[29] B.N. Shivananju, S. Yamdagni, R. Fazuldeen, A.K.S. Kumar, S.P. Nithin, M.M. Varma, S. Asokan, Highly sensitive carbon nanotubes coated etched fiber bragg grating sensor for humidity sensing, IEEE Sens. J. 14 (8) (2014) 2615–2619, https://doi.org/10.1109/JSEN.2014.2312353.
[30] G. Berruti, M. Consales, M. Giordano, L. Sansone, P. Petagna, S. Buontempo, G. Breglio, A. Cusano, Radiation hard humidity sensors for high energy physics applications using polyimide-coated fiber Bragg gratings sensors, Sens. Actuators B Chem. 177 (2013) 94–102, https://doi.org/10.1016/j.snb.2012.10.047.
[31] A.J. Swanson, S.G. Raymond, S. Janssens, R.D. Breukers, M.D.H. Bhuiyan, J.W. Lovell-Smith, M.R. Waterland, Investigation of polyimide coated fibre Bragg gratings for relative humidity sensing, Meas. Sci. Technol. 26 (12) (2015) 125001–127002, https://doi.org/10.1088/0957-0233/26/12/125101.
[32] L. Zhang, F. Gu, J. Lou, X. Yin, L. Tong, Fast detection of humidity with a sub-wavelength-diameter fiber taper coated with gelatin film, Opt. Express 16 (17) (2008) 13349–13353, https://doi.org/10.1364/OE.16.013349.
[33] J.M. Corres, F.J. Arregui, I.R. Matias, Design of humidity sensors based on tapered optical fibers, J. Light. Technol. 24 (11) (2006) 4329–4336, https://doi.org/10.1109/JLT.2006.883668.
[34] J.M. Corres, F.J. Arregui, I.R. Matías, Sensitivity optimization of tapered optical fiber humidity sensors by means of tuning the thickness of nanostructured sensitive coatings, Sens. Actuators B Chem. 122 (2) (2007) 442–449, https://doi.org/10.1016/j.snb.2006.06.008.
[35] J. Mathew, Y. Semenova, G. Rajan, G. Farrell, Humidity sensor based on photonic crystal fibre interferometer, Electron. Lett. 46 (19) (2010) 1341–1343, https://doi.org/10.1049/el.2010.2080.
[36] T. Li, X. Dong, C.C. Chan, K. Ni, S. Zhang, P.P. Shum, Humidity sensor with a PVA-coated photonic crystal fiber interferometer, IEEE Sens. J. 13 (6) (2013) 2214–2216, https://doi.org/10.1109/JSEN.2012.2234100.
[37] D. Lopez-Torres, C. Elosua, J. Villatoro, J. Zubia, M. Rothhardt, K. Schuster, F.J. Arregui, Photonic crystal fiber interferometer coated with a PAH/PAA nanolayer as humidity sensor, Sens. Actuators B Chem. 242 (2017) 1065–1072, https://doi.org/10.1016/J.SNB.2016.09.144.
[38] Y. Wang, C. Shen, W. Lou, F. Shentu, Fiber optic humidity sensor based on the graphene oxide/PVA composite film, Opt. Commun. 372 (2016) 229–234, https://doi.org/10.1016/j.optcom.2016.04.030.

[39] J. An, Y. Jin, M. Sun, X. Dong, Relative humidity sensor based on SMS fiber structure with two waist-enlarged tapers, IEEE Sens. J. 14 (8) (2014) 2683–2686, https://doi.org/10.1109/JSEN.2014.2313878.
[40] M. Consales, A. Buosciolo, A. Cutolo, G. Breglio, A. Irace, S. Buontempo, P. Petagna, M. Giordano, A. Cusano, Fiber optic humidity sensors for high-energy physics applications at CERN, Sens. Actuators B Chem. 159 (1) (2011) 66–74, https://doi.org/10.1016/j.snb.2011.06.042.
[41] M.Y. Mohd Noor, N.M. Kassim, A.S.M. Supaat, M.H. Ibrahim, A.I. Azmi, A.S. Abdullah, G.D. Peng, Temperature-insensitive photonic crystal fiber interferometer for relative humidity sensing without hygroscopic coating, Meas. Sci. Technol. 24 (10) (2013) 102001–107002, https://doi.org/10.1088/0957-0233/24/10/105205.
[42] M.R.K. Soltanian, A.S. Sharbirin, M.M. Ariannejad, I.S. Amiri, R.M. De La Rue, G. Brambilla, B.M.A. Rahman, K.T.V. Grattan, H. Ahmad, Variable waist-diameter mach-zehnder tapered-fiber interferometer as humidity and temperature sensor, IEEE Sens. J. 16 (15) (2016) 5987–5992, https://doi.org/10.1109/JSEN.2016.2573961.
[43] C. Huang, W. Xie, D. Lee, C. Qi, M. Yang, M. Wang, J. Tang, Optical Fiber humidity sensor with porous TiO2/SiO2/TiO2 coatings on Fiber tip, Ieee Photonics Technol. Lett. 27 (14) (2015) 1495–1498, https://doi.org/10.1109/LPT.2015.2426726.
[44] F. Mitschke, Fiber-optic sensor for humidity, Opt. Lett. 14 (17) (1989) 967–969, https://doi.org/10.1364/OL.14.000967.
[45] F.J. Arregui, Y. Liu, I.R. Matias, R.O. Claus, Optical fiber humidity sensor using a nano Fabry-Perot cavity formed by the ionic self-assembly method, Sensors and Actuators, B: Chemical. 59 (1) (1999) 54–59, https://doi.org/10.1016/S0925-4005(99)00232-4.
[46] M. Yang, J. Peng, T. Sun, W. Wang, Y. Qu, Thin-film-based optical fiber Fabry–Perot interferometer used for humidity sensing, Appl. Opt. 57 (12) (2018) 2967–2972, https://doi.org/10.1364/ao.57.002967.
[47] J. Shi, D. Xu, W. Xu, Y. Wang, C. Yan, C. Zhang, D. Yan, Y. He, L. Tang, W. Zhang, T. Liu, J. Yao, Humidity Sensor Based on Fabry-Perot Interferometer and Intracavity Sensing of Fiber Laser, J. Light. Technol. 35 (21) (2017) 4789–4795, https://doi.org/10.1109/JLT.2017.2750172.
[48] J.S. Santos, I.M. Raimundo, C.M.B. Cordeiro, C.R. Biazoli, C.A.J. Gouveia, P.A.S. Jorge, Characterisation of a Nafion film by optical fibre Fabry-Perot interferometry for humidity sensing, Sens. Actuators B Chem. 196 (2014) 99–105, https://doi.org/10.1016/j.snb.2014.01.101.
[49] C.-L. Lee, Y.-W. You, J.-H. Dai, J.-M. Hsu, J.-S. Horng, Hygroscopic polymer microcavity fiber Fizeau interferometer incorporating a fiber Bragg grating for simultaneously sensing humidity and temperature, Sens. Actuators B Chem. 222 (2016) 339–346, https://doi.org/10.1016/j.snb.2015.08.086.
[50] S. Wu, G. Yan, Z. Lian, X. Chen, B. Zhou, S. He, An open-cavity Fabry-Perot interferometer with PVA coating for simultaneous measurement of relative humidity and temperature, Sens. Actuators B Chem. 225 (2016) 50–56, https://doi.org/10.1016/j.snb.2015.11.015.
[51] L.H. Chen, T. Li, C.C. Chan, R. Menon, P. Balamurali, M. Shaillender, B. Neu, X.M. Ang, P. Zu, W.C. Wong, K.C. Leong, Chitosan based fiber-optic Fabry–Perot humidity sensor, Sens. Actuators B Chem. 169 (2012) 167–172, https://doi.org/10.1016/j.snb.2012.04.052.
[52] A. Lopez Aldaba, D. Lopez-Torres, C. Elosua, J.L. Auguste, R. Jamier, P. Roy, F.J. Arregui, M. Lopez-Amo, SnO_2-MOF-Fabry-Perot optical sensor for relative humidity measurements, Sens. Actuators B Chem. 257 (2018) 189–199, https://doi.org/10.1016/j.snb.2017.10.149.
[53] B. Wang, J. Tian, L. Hu, Y. Yao, High sensitivity humidity fiber-optic sensor based on all-agar fabry–Perot interferometer, IEEE Sens. J. 18 (12) (2018) 4879–4885, https://doi.org/10.1109/JSEN.2018.2828134.
[54] O. Arrizabalaga, G. Durana, J. Zubia, J. Villatoro, Accurate microthermometer based on off center polymer caps onto optical fiber tips, Sens. Actuators B Chem. 272 (2018) 612–617, https://doi.org/10.1016/j.snb.2018.05.148.
[55] Y. St-Amant, D. Gariépy, D. Rancourt, Intrinsic properties of the optical coupling between axisymmetric Gaussian beams, Appl. Opt. 43 (30) (2004) 5691–5704, https://doi.org/10.1364/AO.43.005691.
[56] P.R. Wilkinson, J.R. Pratt, Analytical model for low finesse, external cavity, fiber Fabry–Perot interferometers including multiple reflections and angular misalignment, Appl. Opt. 50 (23) (2011) 4671–4680, https://doi.org/10.1364/AO.50.004671.
[57] D. Su, X. Qiao, Q. Rong, H. Sun, J. Zhang, Z. Bai, Y. Du, D. Feng, Y. Wang, M. Hu, Z. Feng, A fiber Fabry–Perot interferometer based on a PVA coating for humidity measurement, Opt. Commun. 311 (2013) 107–110, https://doi.org/10.1016/J.OPTCOM.2013.08.016.
[58] S. Nemoto, T. Makimoto, Analysis of splice loss in single-mode fibres using a Gaussian field approximation, Opt. Quantum Electron. 11 (5) (1979) 447–457, https://doi.org/10.1007/BF00619826.
[59] G. Baschek, G. Hartwig, F. Zahradnik, Effect of water absorption in polymers at low and high temperatures, Polymer. 40 (12) (1999) 3433–3441, https://doi.org/10.1016/S0032-3861(98)00560-6.